Pulmonary Circulation

WILEY

PVRi | Pulmonary Circulation Open Access

RESEARCH ARTICLE OPEN ACCESS

Differences in Pulmonary Artery Flow Hemodynamics Between PAH and PH-HFpEF: Insights From 4D-Flow CMR

Bong-Joon Kim[1,2] | Jeesoo Lee[3] | Haben Berhane[3] | Benjamin H. Freed[1] | Sanjiv J. Shah[1] | James D. Thomas[1]

[1]Division of Cardiology, Northwestern University, Chicago, Illinois, USA | [2]Division of Cardiology, Kosin University College of Medicine, Busan, Korea | [3]Division of Radiology, Northwestern University, Chicago, Illinois, USA

Correspondence: James D. Thomas (James.Thomas2@nm.org)

Received: 14 October 2024 | **Revised:** 14 November 2024 | **Accepted:** 20 November 2024

Funding: This work was supported in part by the IDP Foundation. Bong-Joon Kim was supported by Kosin University College of Medicine.

Keywords: 4D-flow CMR | heart failure with preserved ejection fraction with pulmonary hypertension | pulmonary arterial hypertension | pulmonary artery flow hemodynamics

ABSTRACT

Pulmonary artery (PA) flow analysis is crucial for understanding the progression of pulmonary hypertension (PH). We hypothesized that PA flow characteristics vary according to PH etiology. In this study, we used 4D flow cardiovascular magnetic resonance imaging (CMR) to compare PA flow velocity and wall shear stress (WSS) between patients with pulmonary arterial hypertension (PAH) and those with heart failure with preserved ejection fraction and pulmonary hypertension (PH-HFpEF). We enrolled 13 PAH and 15 PH-HFpEF patients. All participants underwent echocardiography, 4D flow CMR, and right heart catheterization. We compared right ventricular outflow tract (RVOT) flow and main pulmonary artery (MPA) hemodynamics, including peak velocity and mean and maximum WSS, between groups. PH-HFpEF patients were older and more likely to have hypertension. PAH patients had higher mean PA pressure (47.8 ± 8.8 vs. 32.9 ± 6.9 mmHg, $p < 0.001$) and pulmonary vascular resistance (PVR) (8.6 ± 4.6 vs. 2.6 ± 2.2 wood unit, $p < 0.001$). RVOT systolic notching was more common in PAH patients (8 of 13 vs. 0 of 15), and they had shorter RVOT acceleration time (85.5 ± 20.9 vs. 135.0 ± 21.7 ms, $p < 0.001$). PAH patients had lower MPA Vmax (0.8 ± 0.2 vs. 1.1 ± 0.4 m/s, $p = 0.032$), mean WSS (0.29 ± 0.09 vs. 0.36 ± 0.06 Pa, $p = 0.035$), and maximal WSS (0.99 ± 0.18 vs. 1.21 ± 0.19 Pa, $p = 0.011$). Anterior MPA analysis confirmed lower WSS in PAH patients. PVR was negatively correlated with MPA mean WSS ($r = -0.630$, $p = 0.002$). PAH patients had lower MPA Vmax and lower mean MPA WSS in 4D flow CMR compared to PH-HFpEF patients. These distinct PA flow characteristics suggest that the flow hemodynamics of the PA remodeling process differ depending on the underlying etiology of PH.

1 | Introduction

Pulmonary hypertension (PH) is a hemodynamic condition arising from various pathogenic etiologies and associated diseases [1, 2]. Regardless of PH classification, all PH patients have a poor prognosis compared to the general population, including even those with mild or borderline PH [3–5]. The crucial pathologic change in PH is an increase in pulmonary vascular resistance (PVR) caused by vasoconstriction, proliferative remodeling, or occlusion of the pulmonary artery (PA) vasculature [6]. These changes affect the remodeling of PA. If such changes progress, right ventricle (RV)-PA coupling is disrupted beyond RV adaptation, ultimately increasing the risk of death due to RV failure [7]. PH subtypes are differentiated by hemodynamic indices such as mean PA pressure and pulmonary capillary wedge pressure (PCWP), with distinct mechanisms

of PA remodeling depending on PH etiology [2]. Pulmonary arterial hypertension (PAH), classified as Group 1 PH, is defined by a mean PA pressure >20 mmHg, precapillary PH with PCWP ≤ 15 mmHg, and PVR >2 Wood units (WU) [1, 2]. PAH involves distal PA remodeling, increased PVR, reduced compliance, and elevated PA pressure [8]. Group 2 PH, or PH due to left heart disease (LHD), is defined by a mean PA pressure >20 mmHg and PCWP ≥ 15 mmHg. It accounts for most cases of PH, with many patients meeting the diagnosis of HF with preserved ejection fraction (HFpEF). These patients (PH-HFpEF) can be subdivided into isolated post-capillary PH (IpcPH) and combined pre- and post-capillary PH (CpcPH), with CpcPH indicating advanced PA remodeling [9]. While these subtypes are distinguishable in advanced disease, early differentiation often requires precise catheterization.

Blood flow alterations in the PA are crucial for understanding the progression of PH [10–12]. The application of 4D flow cardiovascular magnetic resonance imaging (4D flow CMR) allows a comprehensive assessment of blood flow velocities and characteristics in the PA [13, 14]. This technique also provides physiological vascular parameters, such as wall shear stress (WSS), which are important for understanding vascular remodeling [15, 16]. Due to associated methodological improvements, the technology for analyzing PA flow has become more sophisticated [17]. Many studies have demonstrated the utility of 4D-flow CMR for analyzing RV and PA flow [18–20], as well as its diagnostic performance targeting HFpEF [21, 22]. However, few analyses have examined differences in PA flow features according to PH subtype. Therefore, we hypothesized that PA flow features and WSS differ between PH etiologies. In this study, we compare PA flow hemodynamics in PH-HFpEF and PAH patients using 4D flow CMR.

2 | Methods

2.1 | Study Population

Patients with PH-HFpEF or PAH were prospectively enrolled after undergoing clinically indicated right heart catheterization (RHC) at Northwestern Memorial Hospital. Inclusion criteria for PH-HFpEF were mean PA pressure ≥ 25 mmHg at rest, PCWP ≥ 15 mmHg, LV ejection fraction (LVEF) $\geq 55\%$, and signs/symptoms of HF as defined by Framingham criteria in the last 12 months. Inclusion criteria for PAH were mean PA pressure of ≥ 25 mmHg at rest, and PCWP <15 mmHg. Exclusion criteria included the presence of greater than moderate valvular disease, World Health Organization Groups III–V PH, previous cardiac or pulmonary transplantation, previous history of reduced LVEF $<40\%$, implantable cardioverter defibrillator or pacemaker implantation, claustrophobia, other contraindications to MRI, or glomerular filtration rate <30 mL/min/1.73 m^2. All study participants provided written informed consent, and the institutional review board at Northwestern University approved the study.

2.2 | Comprehensive Echocardiography

All subjects underwent comprehensive 2-dimensional echocardiography with Doppler and tissue Doppler imaging (TDI) using commercially available ultrasound systems with harmonic imaging (Phillips iE33 or 7500; Phillips Medical Systems, Andover, MA, USA; or Vivid 7; GE Healthcare, General Electric Corp., Waukesha, WI, USA) if clinically indicated. Each test was performed with the patient in the left lateral decubitus position. Blood pressure was recorded at the time of echocardiography using a digital blood pressure monitor (Omron HEM-907XL; Omron Healthcare Inc., Vernon Hills, IL, USA). Cardiac structure and function were quantified as recommended by the American Society of Echocardiography [23, 24].

We obtained RV end-diastolic and end-systolic area, basal diameter, and fractional area change, using 2-dimensional echocardiography; tricuspid annular plane systolic excursion (TAPSE) was measured using M-mode and RV myocardial systolic excursion TDI velocity (s′) was obtained according to the American Society of Echocardiography [24]. Pulmonary artery systolic pressure (PASP) and right atrial (RA) pressure were derived as previously described [24]. The presence of systolic notching pattern, RV ejection time (ET), acceleration time (AT), and deceleration time were evaluated on pulse waved (PW) Doppler images from the RV outflow tract (RVOT) flow using the TomTec program (Unterschleißheim, Germany). A single reader trained in quantitative echocardiographic analysis, blinded to all other study data, systematically analyzed all echocardiographic images.

2.3 | RHC

RHC was performed on all PH subjects using either the right internal jugular or right femoral vein approach, employing a standard, fluoroscopy-guided Seldinger technique. Invasive hemodynamics measurements were obtained using a fluid-filled, 6-Fr PA catheter (Edwards Lifesciences, Irvine, CA, USA) and a properly zeroed pressure transducer. Pressure recordings were analyzed offline using a WITT Hemodynamic Workstation (Philips Medical Systems) at a 50 mm/s paper speed, with adjustment of pressure (mmHg) scale as needed. Hemodynamic pressure measurement protocols were standardized, obtained in duplicate at end-expiration, and performed by a physician blinded to all clinical data.

2.4 | Cardiovascular Magnetic Resonance Protocol

All scans were performed using a 1.5-T or 3-T MRI scanner (Siemens Medical Systems). Standard delayed enhancement imaging and cine imaging were conducted. All subjects underwent comprehensive CMR at 1.5 T (MAGNETOM Aera; Siemens Healthineers, Erlangen, Germany). Hematocrit and creatinine levels were measured before the scan, and blood pressure and heart rate were recorded before and after CMR acquisition. The total scan time was approximately 70 min. Phase-contrast imaging was used to assess atrioventricular valve inflow and diastolic function with phase-contrast and bright blood cine techniques. Data analysis was performed using Siemens' prototype VVI software, the ARGUS workstation, and Medis QMass software.

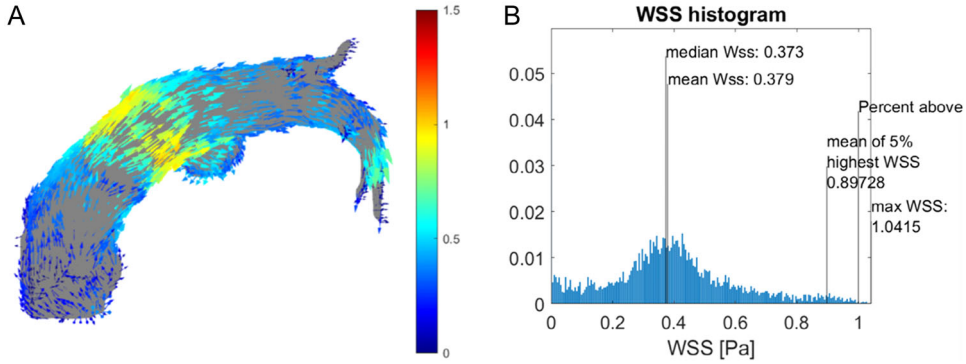

FIGURE 1 | 4D flow MRI images in 61-year-old PAH patient. (A) Maximum intensity projection image of peak systolic WSS of MPA. (B) WSS histogram showing each parameters; mean, median, max 5%, and maximal values of WSS. MPA, main pulmonary artery; MRI, magnetic resonance imaging; Pa, Pascal; PAH, pulmonary arterial hypertension; WSS, wall shear stress.

TABLE 1 | Baseline characteristics.

	PAH ($n = 13$)	PH-HFpEF ($n = 15$)	p value
Age (years)	56.8 ± 14.5	69.9 ± 6.7	0.009
Female sex (%)	10 (76.9)	10 (66.7)	0.686
Body surface area (m^2)	1.8 ± 0.3	2.1 ± 0.3	0.011
Systolic BP (mmHg)	123.4 ± 16.2	138.0 ± 17.4	0.030
Diastolic BP (mmHg)	68.5 ± 11.9	76.1 ± 12.5	0.110
Hypertension (%)	4 (30.8)	12 (80)	0.012
Diabetes mellitus (%)	3 (23.1)	5 (33.3)	0.686
Hyperlipidemia (%)	2 (15.3)	12 (80.0)	0.002
Coronary artery disease (%)	2 (15.4)	7 (46.7)	0.114
Atrial fibrillation (%)	4 (30.8)	4 (26.7)	0.569
Chronic obstructive pulmonary disease (%)	3 (23.1)	5 (33.3)	0.686

Abbreviations: BP, blood pressure; PAH, pulmonary arterial hypertension; PH-HFpEF, pulmonary hypertension with heart failure preserved ejection fraction.

Additionally, all subjects underwent whole-heart, sagittal-oblique 4D flow MRI with respiratory navigator and retrospective ECG gating. The 4D flow data were processed for eddy current correction, noise masking, and velocity aliasing correction using an in-house MATLAB tool [25]. Phase-contrast MR angiograms were generated from the 4D flow CMR and used to segment the PA with commercial software (Mimics; Materialise, Leuven, Belgium). Peak systolic WSS in the MPA was derived in MATLAB using a method described previously (Figure 1A), and the mean, median, max 5%, and maximal values of WSS were measured (Figure 1B) [26]. Additionally, regional mean, median, and max 5% WSS were quantified at anterior and posterior MPA, determined by manually drawn ROIs (Figure S1).

2.5 | Statistical Analysis

Categorical variables were expressed as count and percentages and continuous variables with normal distributions were expressed as mean ± standard deviation. Non-normally distributed continuous variables were reported as medians (25th percentile, 75th percentile). We used Student's *t*-test to compare the means of normally distributed continuous variables between PH-HFpEF and PAH subjects, and the nonparametric Mann–Whitney *U*-test for non-normally distributed variables. Categorical variables were compared using Fisher's exact or χ^2 tests. We examined the correlation between parameters from 4D flow MRI using Pearson pairwise correlation. Two-sided p values < 0.05 were considered significant. All analyses were performed using STATA (Version 17, StataCorp.; College Station, TX, USA).

3 | Results

Among baseline characteristics, PH-HFpEF patients were older, with higher body surface area, and a higher prevalence of hypertension and hyperlipidemia than PAH patients (Table 1). In baseline RHC (Table 2), PAH patients had significantly higher mean PA pressure (47.8 ± 8.8 vs. 32.9 ± 6.9 mmHg, $p < 0.001$) and PVR (8.6 ± 4.6 vs. 2.6 ± 2.2 WU, $p < 0.001$) than PH-HFpEF patients. According to echocardiography, there were no significant differences in RV size, RV fraction area change, TAPSE, or S′ velocity between groups (Table 3). In the analysis of RVOT PW Doppler, 8 PAH patients (61.5%) showed significant systolic notching pattern, compared to none in PH-HFpEF patients. There were no differences in RVOT VTI (15.5 ± 3.6 vs. 14.5 ± 3.5 cm, $p = 0.508$) of RVOT ET (359.5 ± 72.8 vs. 386.1 ± 52.4 ms, $p = 0.282$)

TABLE 2 | Invasive right heart catheterization.

	PAH ($n = 12$)	PH-HFpEF ($n = 15$)	p value
RA pressure (mmHg)	8.7 ± 5.0	11.1 ± 4.5	0.193
RVSP (mmHg)	77.2 ± 13.1	48.6 ± 12.7	< 0.001
RVDP (mmHg)	6.8 ± 4.2	7.5 ± 3.4	0.637
PASP (mmHg)	77.1 ± 14.0	47.8 ± 12.9	< 0.001
PADP (mmHg)	29.6 ± 7.7	21.1 ± 4.6	0.002
Mean PAP (mmHg)	47.8 ± 8.8	32.9 ± 6.9	< 0.001
TPG (mmHg)	35.8 ± 8.5	14.2 ± 6.4	< 0.001
DPG (mmHg)	17.7 ± 7.3	3.5 ± 3.2	< 0.001
PCWP (mmHg)	11.9 ± 3.5	18.7 ± 4.2	< 0.001
Cardiac output (L/min)	5.0 ± 1.3	5.4 ± 1.3	0.436
Cardiac index (L/min/m^2)	2.8 ± 0.6	2.7 ± 0.7	0.693
PVR (WU)	8.6 ± 4.6	2.6 ± 2.2	0.001

Abbreviations: DPG, diastolic pulmonary gradient; PADP, pulmonary arterial diastolic pressure; PAH, pulmonary arterial hypertension; PAP, pulmonary arterial pressure; PASP, pulmonary arterial systolic pressure; PCWP, pulmonary capillary wedge pressure; PH-HFpEF, pulmonary hypertension with heart failure preserved ejection fraction; PVR, pulmonary vascular resistance; RA, right atrium; RVDP, right ventricle diastolic pressure; RVSP, right ventricle systolic pressure; TPG, transpulmonary gradient; WU, wood unit.

TABLE 3 | Echocardiographic data.

	PAH ($n = 13$)	PH-HFpEF ($n = 15$)	p value
LV ejection fraction (%)	68.1 ± 7.2	61.4 ± 11.9	0.092
LVEDD (mm)	32.7 ± 16.9	41.0 ± 16.5	0.198
LVESD (mm)	20.6 ± 10.9	27.7 ± 12.3	0.119
E/A ratio	1.1 ± 0.4	1.3 ± 0.7	0.416
E/E′	12.4 ± 3.9	12.5 ± 4.9	0.954
LA volume index (mL/m^2)	24.3 ± 3.7	38.6 ± 18.2	0.010
RV FAC (%)	37.6 ± 9.0	38.2 ± 9.8	0.859
TAPSE (cm)	2.3 ± 0.4	2.1 ± 0.6	0.303
RV S′ (cm/s)	11.9 ± 1.2	11.2 ± 1.8	0.406
RVOT Vmax (m/s)	0.75 ± 0.17	0.67 ± 0.15	0.206
RVOT Vmean (m/s)	0.47 ± 0.09	0.46 ± 0.10	0.673
RVOT max PG (mmHg)	2.3 ± 1.0	1.8 ± 0.8	0.179
RVOT mean PG (mmHg)	1.2 ± 0.4	1.0 ± 0.5	0.426
RVOT VTI (cm)	15.5 ± 3.6	14.5 ± 3.5	0.508
RVOT systolic notching pattern	8 (61.5%)	0 (0%)	0.001
RVOT ejection time (msec)	359.5 ± 72.8	386.1 ± 52.4	0.282
RVOT acceleration time (msec)	85.5 ± 20.9	135.0 ± 21.7	< 0.001
RVOT deceleration time (msec)	265.5 ± 46.6	245.2 ± 51.0	0.303
AT/ET ratio	0.24 ± 0.04	0.35 ± 0.05	< 0.001

Note: Normal reference values of parameters (abnormal threshold) – RV FAC (%): 49 ± 7 (< 35), TAPSE (cm): 2.4 ± 0.4 (< 1.7), RV S′ (cm/s): 14.1 ± 2.3 (< 9.5), RVOT acceleration time [27] (msec): 138.7 ± 17.5.
Abbreviations: A, peak late diastolic mitral filling velocity; AT, acceleration time; E, peak early diastolic mitral filling velocity; E′, early diastolic mitral annular velocity; ET, ejection time; LV, left ventricle; LVEDD, Left ventricle end-diastolic dimension; LVESD, left ventricle end-systolic dimension; PAH, pulmonary arterial hypertension; PH-HFpEF, pulmonary hypertension with heart failure preserved ejection fraction; PG, pressure gradient; PW, pulse waved; RV, right ventricle; RVOT, right ventricle outflow tract; TAPSE, tricuspid annular plane systolic excursion; VTI, velocity time integral.

between groups. However, PAH patients showed significantly shorter AT of RVOT flow (85.5 ± 20.9 vs. 135.0 ± 21.7 ms, $p < 0.001$) and lower AT/ET ratio (0.24 ± 0.04 vs. 0.35 ± 0.05, $p < 0.001$) than PH-HFpEF patients.

In analysis of 4D-flow CMR data (Table 4), PAH and PH-HFpEF patients exhibited similar MPA vorticity and helicity. However, PAH patients had significantly lower MPA Vmax compared to PH-HFpEF (0.8 ± 0.2 vs. 1.1 ± 0.4 m/s, $p = 0.032$) (Figure 2A). PAH

TABLE 4 | 4D flow MRI parameters of main pulmonary artery.

	PAH ($n = 13$)	PH-HFpEF ($n = 15$)	p value
MPA Vmax (m/s)	0.8 ± 0.2	1.1 ± 0.4	0.032
MPA net flow (mL/cycle)	63.45 ± 22.9	78.9 ± 19.9	0.067
MPA forward flow (mL/cycle)	64.8 ± 22.2	80.5 ± 20.1	0.060
MPA retrograde flow (mL/cycle)	−1.4 ± 2.3	−1.6 ± 1.9	0.748
MPA area systolic (cm^2)	11.2 ± 3.2	9.0 ± 2.5	0.126
MPA area diastolic (cm^2)	9.4 ± 2.9	7.4 ± 2.5	0.134
MPA vorticity (s^{-1})	2.0 ± 0.6	1.8 ± 0.6	0.362
MPA helicity (m^2w^2)	1.5 ± 0.9	1.3 ± 0.5	0.464
MPA WSS max (Pa)	0.99 ± 0.18	1.21 ± 0.19	0.011
MPA WSS mean (Pa)	0.29 ± 0.09	0.36 ± 0.06	0.035
Anterior	0.34 ± 0.10	0.43 ± 0.13	0.049
Posterior	0.39 ± 0.11	0.46 ± 0.10	0.133
MPA WSS median (Pa)	0.28 ± 0.09	0.34 ± 0.07	0.105
Anterior	0.32 ± 0.10	0.42 ± 0.14	0.055
Posterior	0.42 ± 0.10	0.43 ± 0.12	0.746
MPA WSS max 5% (Pa)	0.74 ± 0.19	0.88 ± 0.12	0.055
Anterior	0.69 ± 0.18	0.90 ± 0.19	0.009
Posterior	0.77 ± 0.20	0.91 ± 0.18	0.055

Abbreviations: MPA, main pulmonary artery; MRI, magnetic resonance imaging; Pa, Pascal; PAH, pulmonary arterial hypertension; PH-HFpEF, pulmonary hypertension with heart failure preserved ejection fraction; WSS, wall shear stress.

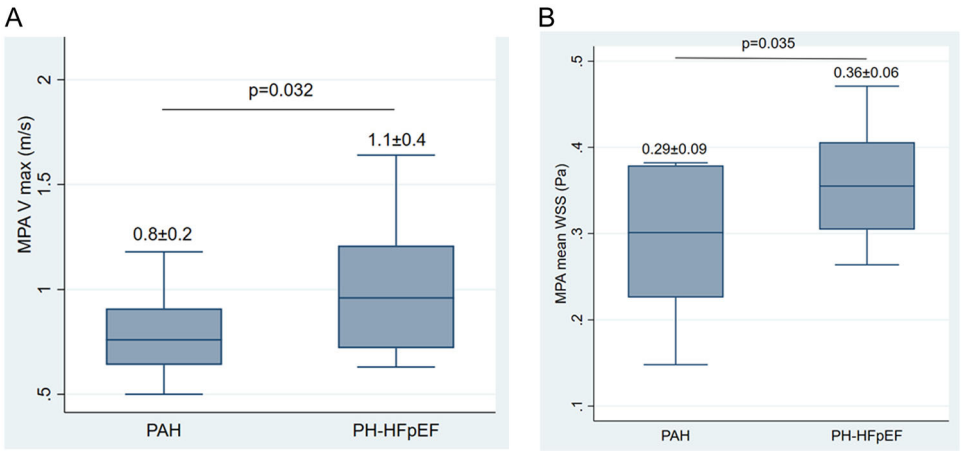

FIGURE 2 | (A) MPA Vmax of PAH and PH-HFpEF. (B) Mean MPA WSS in PAH and PH-HFpEF. MPA, main pulmonary artery; Pa, Pascal; PAH, pulmonary arterial hypertension; PH-HFpEF, pulmonary hypertension with heart failure preserved ejection fraction; WSS, wall shear stress.

patients showed a trend of larger MPA area than HFpEF, although this difference was not statistically significant (MPA area systolic: 11.2 ± 3.2 vs. 9.0 ± 2.5 cm^2, $p = 0.126$ and MPA area diastolic: 9.4 ± 2.9 vs. 7.4 ± 2.5 cm^2, $p = 0.134$). In the analysis of WSS of MPA, PAH patients had significantly lower mean WSS (0.29 ± 0.09 vs. 0.36 ± 0.06 Pa, $p = 0.035$) (Figure 2B) and max WSS (0.99 ± 0.18 vs. 1.21 ± 0.19 Pa, $p = 0.011$) compared to PH-HFpEF patients. When we analyzed WSS by dividing MPA into anterior and posterior portions, PAH patients had significantly lower mean WSS (0.34 ± 0.10 vs. 0.43 ± 0.13 Pa, $p = 0.049$) and max 5% WSS (0.69 ± 0.18 vs. 0.90 ± 0.19 Pa, $p = 0.009$) in the anterior portion, but the difference was not statistically significant in the posterior portion. In Pearson correlation analysis between PVR on RHC and 4D flow MRI parameters, the mean WSS of MPA had a significantly negative correlation with PVR ($r = -0.630$, $p = 0.002$) (Figure 3).

4 | Discussion

WSS is a dynamic frictional force induced by blood flow along the surface of the vascular walls [11]. WSS has long been used to assess vascular characteristics [28] and is correlated with markers of stiffness and elasticity in the PA [29]. In our results, MPA Vmax and mean WSS were significantly lower in PAH

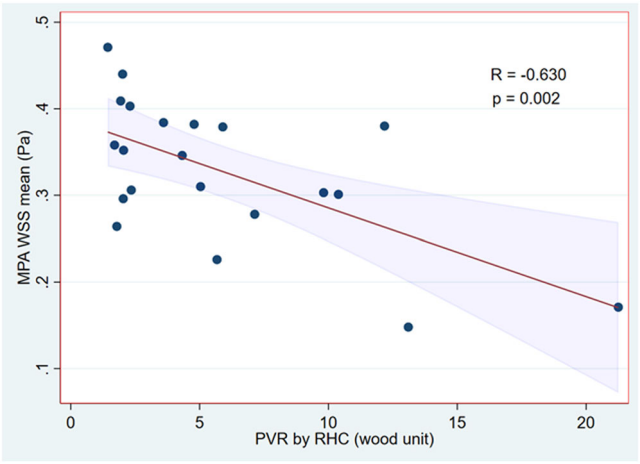

FIGURE 3 | Scatter plot with Pearson correlation of mean MPA WSS and PVR. MPA, main pulmonary artery; PVR, pulmonary vascular resistance; RHC, right heart catheterization; WSS, wall shear stress.

patients compared to PH-HFpEF patients, with negative correlations between MPA mean WSS and PVR. These findings align with RHC and echocardiography results, showing higher PVR, more notching patterns, and altered RVOT flow in PAH patients. These changes are well-known indicators of pulmonary vascular load and RV function [30].

In PAH progression, increased afterload, along with disturbances in autonomic tone and myocardial perfusion mismatch, drive pathological changes in cardiomyocyte structure and function. These changes heighten RV stiffness and impair contractility, leading to RA and RV dilation, and TR [31]. Due to RV-PA interaction, alterations in PA flow may occur directly. In several previous studies, PAH patients showed significantly lower WSS in PA compared to healthy controls [32, 33]. These results are likely because WSS theoretically represents changes in PA well in terms of the progression of PAH. In contrast, in PH-HFpEF, PA pressure increases slowly due to the accumulation of mechanical factors such as volume overload over long periods of time accompanying underlying diseases or aging [9, 34], so changes in PA may be relatively small. This difference in mechanism may explain variation in blood flow in the PA and may affect remodeling of the PA. Thus, our findings confirmed that completely different forms of PA remodeling are observed in PAH and PH-HFpEF due to differences in flow characteristics, and hemodynamically suggest that PAH has greater resistance force preventing normal PA blood flow than PH-HFpEF. Therapeutic approaches to PH-HFpEF have historically targeted volume overload and the underlying LHD. However, in advanced PH-HFpEF with significant PA remodeling, PAH-specific drugs may be beneficial. While studies of PAH drugs in PH-HFpEF have been conducted, significant improvements in outcomes such as survival remain limited [34–36]. If future studies show positive results, PVR could become a key indicator for treatment decisions. Although 4D CMR has not been widely used in PH patients to date, the correlation between WSS and PVR demonstrated in our study suggests that MPA WSS is a noninvasive marker of PVR with both clinical and investigational value.

Interestingly, we found significant differences in WSS in the anterior PA, while the posterior PA WSS remained similar between PAH and PH-HFpEF. Blood flow in the PA is complex, and various factors, including vortex formation and retrograde flow, can affect flow direction [37]. According to a previous study analyzing CMR-derived 3D blood flow patterns in the MPA, specific flow patterns characterize the anterior and posterior walls of the MPA, and the main blood flow is biased toward the anterior wall [19]. In this study, the Vmax of blood flow in the PA differed depending on the position of the PA, and factors such as vortex formation and retrograde flow affected the direction of blood flow in the PA. However, although our study had the advantage of being focused on WSS, the small sample size may have limited our ability to detect differences in other indices like vorticity. The significant differences in PVR and RVOT flow patterns, coupled with the correlation between PVR and WSS, support the hypothesis that PA flow dynamics differ between PAH and PH-HFpEF.

Our study has limitations, including a small patient cohort, which may reduce its statistical power. Additionally, the use of 4D-flow MRI data sets can introduce errors due to factors such as signal noise, vessel size, and magnetic field strength. We only analyzed the pattern of PA flow, which could not analyze changes at the cellular level, which limits our ability to explain overall PA remodeling. Despite these limitations, our study is the first to reveal distinct flow dynamics, including MPA WSS, between PAH and PH-HFpEF using 4D flow CMR. While we cannot definitively conclude whether PA remodeling leads to changes in flow or vice versa, our findings support the hypothesis that PA remodeling varies by PH etiology. Future studies could further investigate the implications of PA flow dynamics on the clinical outcomes of various PH patients.

5 | Conclusion

PAH and PH-HFpEF exhibit distinct PA flow dynamics on 4D flow CMR. PAH patients show lower MPA Vmax and mean WSS compared to PH-HFpEF patients, and MPA mean WSS is significantly correlated with PVR. These findings suggest that the PA remodeling processes differ by PH etiology, with MPA WSS potentially serving as a novel indicator of PA remodeling in PH patients.

Author Contributions

Bong-Joon Kim, Jeesoo Lee, and James D. Thomas made substantial contributions to the conception and design of the study. Data collection was conducted by Benjamin H. Freed and Sanjiv J. Shah. Jeesoo Lee and Haben Berhane generated and analyzed the 4D MRI images. Data analysis was performed by Bong-Joon Kim, while James D. Thomas, Jeesoo Lee, and Bong-Joon Kim contributed to data interpretation. Bong-Joon Kim prepared the original draft, with all other authors involved in drafting and revising the manuscript. James D. Thomas conducted the final review and editing.

Acknowledgments

Dr. James D. Thomas acts as the guarantor for this manuscript and accepts full responsibility for the work, ensuring that the integrity and accuracy of the research are maintained. Dr. James D. Thomas confirms that all authors have seen and approved the final version of the

manuscript and have agreed to its submission for publication. This work was supported in part by the IDP Foundation. Bong-Joon Kim was supported by Kosin University College of Medicine.

Ethics Statement

All study participants provided written informed consent, and the institutional review board at Northwestern University approved the study.

Conflicts of Interest

The authors declare no conflicts of interest.

Data Availability Statement

The data that support the findings of this study are available from the corresponding author upon reasonable request.

References

1. M. Humbert, G. Kovacs, M. M. Hoeper, et al., "2022 ESC/ERS Guidelines for the Diagnosis and Treatment of Pulmonary Hypertension," *European Heart Journal* 43, no. 38 (2022): 3618–3731.

2. G. Kovacs, S. Bartolome, C. P. Denton, et al., "Definition, Classification and Diagnosis of Pulmonary Hypertension," *European Respiratory Journal* 64 (2024): 2401324.

3. G. Strange, S. Stewart, D. S. Celermajer, et al., "Threshold of Pulmonary Hypertension Associated With Increased Mortality," *Journal of the American College of Cardiology* 73, no. 21 (2019): 2660–2672.

4. B. A. Maron, E. Hess, T. M. Maddox, et al., "Association of Borderline Pulmonary Hypertension With Mortality and Hospitalization in a Large Patient Cohort: Insights From the Veterans Affairs Clinical Assessment, Reporting, and Tracking Program," *Circulation* 133, no. 13 (2016): 1240–1248.

5. N. Karia, L. Howard, M. Johnson, et al., "Predictors of Outcomes in Mild Pulmonary Hypertension According to 2022 ESC/ERS Guidelines: The EVIDENCE-PAH UK Study," *European Heart Journal* 44, no. 44 (2023): 4678–4691.

6. J. Omura, S. Bonnet, and S. Kutty, "Right Ventricular and Pulmonary Vascular Changes in Pulmonary Hypertension Associated With Left Heart Disease," *American Journal of Physiology-Heart and Circulatory Physiology* 316, no. 5 (2019): H1144–H1145.

7. Z. A. Rako, N. Kremer, A. Yogeswaran, M. J. Richter, and K. Tello, "Adaptive Versus Maladaptive Right Ventricular Remodelling," *ESC Heart Failure* 10, no. 2 (2023): 762–775.

8. D. G. Kiely, D. Levin, P. Hassoun, et al., "EXPRESS: Statement on Imaging and Pulmonary Hypertension From the Pulmonary Vascular Research Institute (PVRI)," *Pulmonary Circulation* 9, no. 3 (2019): 2045894019841990.

9. A. Y. Jang, S. J. Park, and W. J. Chung, "Pulmonary Hypertension in Heart Failure," *International Journal of Heart Failure* 3, no. 3 (2021): 147–159.

10. S. Mosbahi, E. Mickaily-Huber, D. Charbonnier, et al., "Computational Fluid Dynamics of the Right Ventricular Outflow Tract and of the Pulmonary Artery: A Bench Model of Flow Dynamics," *Interactive Cardiovascular and Thoracic Surgery* 19, no. 4 (2014): 611–616.

11. B. T. Tang, S. S. Pickard, F. P. Chan, P. S. Tsao, C. A. Taylor, and J. A. Feinstein, "Wall Shear Stress Is Decreased in the Pulmonary Arteries of Patients With Pulmonary Arterial Hypertension: An Image-Based, Computational Fluid Dynamics Study," *Pulmonary Circulation* 2, no. 4 (2012): 470–476.

12. H. H. Wang, W. Y. I. Tseng, H. Y. Yu, M. C. Chang, and H. H. Peng, "Phase-Contrast Magnetic Resonance Imaging for Analyzing Hemodynamic Parameters and Wall Shear Stress of Pulmonary Arteries in Patients With Pulmonary Arterial Hypertension," *Magnetic Resonance Materials in Physics, Biology and Medicine* 32, no. 6 (2019): 617–627.

13. M. Markl, P. J. Kilner, and T. Ebbers, "Comprehensive 4D Velocity Mapping of the Heart and Great Vessels by Cardiovascular Magnetic Resonance," *Journal of Cardiovascular Magnetic Resonance* 13, no. 1 (2011): 7.

14. J. P. Alunni, B. Degano, C. Arnaud, et al., "Cardiac MRI in Pulmonary Artery Hypertension: Correlations Between Morphological and Functional Parameters and Invasive Measurements," *European Radiology* 20, no. 5 (2010): 1149–1159.

15. U. Gülan, V. A. Rossi, A. Gotschy, et al., "A Comparative Study on the Analysis of Hemodynamics in the Athlete's Heart," *Scientific Reports* 12, no. 1 (2022): 16666.

16. Z. Wang, R. S. Lakes, M. Golob, J. C. Eickhoff, and N. C. Chesler, "Changes in Large Pulmonary Arterial Viscoelasticity in Chronic Pulmonary Hypertension," *PLoS One* 8, no. 11 (2013): e78569.

17. K. Lin, R. Sarnari, D. Z. Gordon, M. Markl, and J. C. Carr, "Cine MRI-Derived Radiomics Features Indicate Hemodynamic Changes in the Pulmonary Artery," *International Journal of Cardiovascular Imaging* 40, no. 2 (2024): 287–294.

18. K. Odagiri, N. Inui, A. Hakamata, et al., "Non-Invasive Evaluation of Pulmonary Arterial Blood Flow and Wall Shear Stress in Pulmonary Arterial Hypertension With 3D Phase Contrast Magnetic Resonance Imaging," *SpringerPlus* 5, no. 1 (2016): 1071.

19. G. Reiter, U. Reiter, G. Kovacs, et al., "Magnetic Resonance-Derived 3-Dimensional Blood Flow Patterns in the Main Pulmonary Artery as a Marker of Pulmonary Hypertension and a Measure of Elevated Mean Pulmonary Arterial Pressure," *Circulation: Cardiovascular Imaging* 1, no. 1 (2008): 23–30.

20. H. Gbinigie, L. Coats, J. D. Parikh, K. G. Hollingsworth, and L. Gan, "A 4D Flow Cardiovascular Magnetic Resonance Study of Flow Asymmetry and Haemodynamic Quantity Correlations in the Pulmonary Artery," *Physiological Measurement* 42, no. 2 (2021): 025005.

21. C. T. Kwan, O. H. S. Ching, P. M. Yap, et al., "Intraventricular 4D Flow Cardiovascular Magnetic Resonance for Assessing Patients With Heart Failure With Preserved Ejection Fraction: A Pilot Study," *International Journal of Cardiovascular Imaging* 39, no. 10 (2023): 2015–2027.

22. H. Ota, H. Kamada, S. Higuchi, and K. Takase, "Clinical Application of 4D Flow MR Imaging to Pulmonary Hypertension," *Magnetic Resonance in Medical Sciences* 21, no. 2 (2022): 309–318.

23. S. F. Nagueh, C. P. Appleton, T. C. Gillebert, et al., "Recommendations for the Evaluation of Left Ventricular Diastolic Function by Echocardiography," *Journal of the American Society of Echocardiography* 22, no. 2 (2009): 107–133.

24. L. G. Rudski, W. W. Lai, J. Afilalo, et al., "Guidelines for the Echocardiographic Assessment of the Right Heart in Adults: A Report From the American Society of Echocardiography Endorsed by the European Association of Echocardiography, a Registered Branch of the European Society of Cardiology, and the Canadian Society of Echocardiography," *Journal of the American Society of Echocardiography* 23, no. 7 (2010): 685–713.

25. S. Schnell, P. Entezari, R. J. Mahadewia, et al., "Improved Semiautomated 4D Flow MRI Analysis in the Aorta in Patients With Congenital Aortic Valve Anomalies Versus Tricuspid Aortic Valves," *Journal of Computer Assisted Tomography* 40, no. 1 (2016): 102–108.

26. P. van Ooij, W. V. Potters, J. Collins, et al., "Characterization of Abnormal Wall Shear Stress Using 4D Flow MRI in Human Bicuspid Aortopathy," *Annals of Biomedical Engineering* 43, no. 6 (2015): 1385–1397.

27. A. M. Marra, N. Benjamin, F. Ferrara, et al., "Reference Ranges and Determinants of Right Ventricle Outflow Tract Acceleration Time in

Healthy Adults by Two-Dimensional Echocardiography," *International Journal of Cardiovascular Imaging* 33, no. 2 (2017): 219–226.

28. A. M. Malek, "Hemodynamic Shear Stress and Its Role in Atherosclerosis," *Journal of the American Medical Association* 282, no. 21 (1999): 2035–2042.

29. M. Schäfer, V. O. Kheyfets, J. D. Schroeder, et al., "Main Pulmonary Arterial Wall Shear Stress Correlates With Invasive Hemodynamics and Stiffness in Pulmonary Hypertension," *Pulmonary Circulation* 6, no. 1 (2016): 37–45.

30. H. Takahama, R. B. McCully, R. P. Frantz, and G. C. Kane, "Unraveling the RV Ejection Doppler Envelope," *JACC: Cardiovascular Imaging* 10, no. 10, Pt. B (2017): 1268–1277.

31. A. R. Hemnes, D. S. Celermajer, M. D'Alto, et al., "Pathophysiology of the Right Ventricle and Its Pulmonary Vascular Interaction," *European Respiratory Journal* 64 (2024): 2401321.

32. A. J. Barker, A. Roldán-Alzate, P. Entezari, et al., "Four-Dimensional Flow Assessment of Pulmonary Artery Flow and Wall Shear Stress in Adult Pulmonary Arterial Hypertension: Results From Two Institutions," *Magnetic Resonance in Medicine* 73, no. 5 (2015): 1904–1913.

33. M. Terada, Y. Takehara, H. Isoda, T. Uto, M. Matsunaga, and M. Alley, "Low WSS and High OSI Measured by 3D Cine PC MRI Reflect High Pulmonary Artery Pressures in Suspected Secondary Pulmonary Arterial Hypertension," *Magnetic Resonance in Medical Sciences* 15, no. 2 (2016): 193–202.

34. B. A. Maron, G. Bortman, T. De Marco, et al., "Pulmonary Hypertension Associated With Left Heart Disease," *European Respiratory Journal* 64 (2024): 2401344.

35. J. L. Vachiéry, M. Delcroix, H. Al-Hiti, et al., "Macitentan in Pulmonary Hypertension Due to Left Ventricular Dysfunction," *European Respiratory Journal* 51, no. 2 (2018): 1701886.

36. B. Pieske, A. P. Maggioni, C. S. P. Lam, et al., "Vericiguat in Patients With Worsening Chronic Heart Failure and Preserved Ejection Fraction: Results of the SOluble guanylate Cyclase stimulatoR in heArT failurE patientS With PRESERVED EF (SOCRATES-PRESERVED) Study," *European Heart Journal* 38, no. 15 (2017): 1119–1127.

37. U. Reiter, G. Reiter, G. Kovacs, et al., "Evaluation of Elevated Mean Pulmonary Arterial Pressure Based on Magnetic Resonance 4D Velocity Mapping: Comparison of Visualization Techniques," *PLoS One* 8, no. 12 (2013): e82212.

Supporting Information

Additional supporting information can be found online in the Supporting Information section.